The Effects of Superimposed Hydrostatic Pressure on Deformation and Fracture: Part I. Monolithic 6061 Aluminum

D.S. LIU and J.J. LEWANDOWSKI

The effects of various levels of superimposed hydrostatic pressure on the tensile ductility and fracture micromechanisms were determined for 6061 specimens heat-treated to underaged and overaged conditions of equivalent yield strength. Superimposed pressures of 0.1, 150, and 300 MPa were selected; the ductility increased between 0.1 and 150 MPa and remained constant between 150 and 300 MPa. It is shown that the levels of pressure chosen inhibit void growth and coalescence. Void nucleation occurred at nonmetallic inclusions, and neither the ductility nor pressure response were significantly affected by the heat treatments chosen.

I. INTRODUCTION

IN this symposium on "Quasi-Brittle Fracture," a variety of experimental techniques have been employed to examine the behavior of quasi-brittle materials, including changes in test temperature, loading rate, stress state, and impurity doping. Changing the stress state *via* the introduction of a notch which generates hydrostatic tensile stresses during loading generally produces a drop in ductility and an increase in the ductile-to-brittle transition temperature. However, the effects of superimposed hydrostatic compressive stresses upon tensile ductility of a variety of monolithic materials have also been documented.[1–24] A pressure of sufficient magnitude can significantly enhance the tensile ductility of nominally brittle materials and decrease the ductile-to-brittle transition temperature, as well as extend the ductility of ductile materials. The nature of the ductility-pressure relationship varies considerably between materials and heat treatments (*i.e.*, *microstructures*), while the following effects of superimposed hydrostatic pressure on the mechanical behavior of monolithic materials have been proposed:

(1) ductility enhancement *via* the suppression of fracture (*e.g.*, microvoid) nucleation,[1–5] growth,[1,6,7,19] or coalescence[1,6,7,19] of fractured nuclei (*e.g.*, microvoid coalescence);
(2) flow stress increases[9–11] and increasing work-hardening rate,[8,12] proposed as due to pressure-induced decreases in the density and mobility of dislocations;[8–12] and
(3) pressure-induced injection of dislocations at second-phase particles,[15–18,21,25–27] producing changes in flow stress and ductility enhancement in some quasi-brittle systems such as Cr,[15–18] metal-matrix composites (*e.g.*, Al/SiCp),[25] and NiAl.[21,26–28]

In recent years, metal-matrix composites have received great commercial interest because they offer the potential of improved strength and modulus, high strength-to-weight ratio, and rigidity at high temperature for use in specialized applications. The parameters influencing the mechanical properties of composite materials are complex and interrelated, while the prime factors are matrix alloy, interfacial bonding, reinforcement content, reinforcement size, and morphology and distribution of the reinforcement.[22,29–31] It is often observed that increasing the reinforcement loading produces a decrease in ductility, while the mechanisms of fracture initiation and growth and their effect on the ductility in discontinuously reinforced materials are under discussion.[22–25,29–35] Since the characteristics of reduced ductility are closely associated with the yielding and flow characteristics in metal-matrix composites, studies on the yielding and flow mechanisms at ambient temperature are necessary to understand the basic parameters which control fracture. However, the plastic behavior at moderate strains cannot normally be studied in tension in these metal-matrix composites at room temperature because of their relatively low ductility. A number of experimental techniques have been utilized in an attempt to study the micromechanisms of deformation and fracture in composite materials exhibiting little macroscopic tensile ductility. The enhancement of ductility by superimposed hydrostatic pressure, however, provides an important means of studying the fracture micromechanisms in these materials, as well as providing an experimental technique to evaluate the role of hydrostatic stresses in the fracture of these materials.

There has been relatively little work[22–25,29,32,33] on determining the effects of superimposed hydrostatic pressure on the behavior of metal-matrix composites. The potential void-nucleating features in aluminum alloy composites include the reinforcement as well as sites present in the matrix (*e.g.*, precipitates, inclusions, grain boundaries). As such, the present work was conducted to first determine and quantify the effects of different levels of superimposed pressure on the ductility and damage (*i.e.*, void nucleation at inclusions or precipitates) evolution in a 6061 aluminum alloy heat-treated to different aging conditions of equivalent strength, while Part II[36] investigates the effects of pressure on the same alloy reinforced with 15 vol pct Al_2O_3 particulate. In both the monolithic and the composite specimens, heat treatments were designed to produce underaged and overaged

D.S. LIU, Graduate Student, and J.J. LEWANDOWSKI, Associate Professor, are with the Department of Materials Science and Engineering, Case Western Reserve University, Cleveland, OH 44106.

This article is based on a presentation made in the symposium "Quasi-Brittle Fracture" presented during the TMS fall meeting, Cincinnati, OH, October 21–24, 1991, under the auspices of the TMS Mechanical Metallurgy Committee and the ASM/MSD Flow and Fracture Committee.

microstructures of equivalent yield strength, but containing aging particles of very different size and character. Complementary work conducted on intermetallics (*e.g.*, NiAl) is summarized elsewhere.[21,26–28]

II. EXPERIMENTAL PROCEDURES

The 6061 monolithic aluminum alloy was received in the as-extruded condition, while a three-dimensional view of the microstructure is shown in Figure 1. The grain size along the extrusion direction was 10 μm, while a pancake-shaped grain structure is evident. The following heat treatments were selected to produce underaged (UA) and overaged (OA) microstructures possessing equivalent values of yield strength and matrix microhardness: solution treatment at 510 °C/4 hours/water-quenched; artificial aging: 175 °C/2 hours for the UA condition, 175 °C/100 hours for the OA condition. These treatments were chosen based on aging curves developed from microhardness and macrohardness tests of specimens heat-treated for various times at 175 °C. Transmission electron microscope (TEM) thin foils were prepared *via* standard jet polishing techniques using a perchloric acid/methanol solution, while viewing was accomplished on a JEOL 200 TEM operated at 100 KV.

Smooth cylindrical tensile specimens were taken along the extrusion direction and were designed such that the ratio of gage length (15.2 mm) to gage diameter (3.8 mm) was 4 to 1 in accordance with ASTM Standard E8-87a. Specimens were metallographically polished to a mirror finish before testing to permit optical and scanning electron microscopy studies of the surface before and after deformation. Tensile testing was conducted to failure at a constant displacement rate of 0.2 mm/min at atmospheric pressure (*i.e.*, 0.1 MPa) and under constant superimposed hydrostatic pressures of either 150 or 300 MPa. Tensile testing at 0.1 MPa was conducted on an Instron Model 1125 Universal Testing Machine, while those performed under superimposed pressure were conducted in our recently modified high-pressure laboratory.[21–29] Axial strain in the tests conducted at 0.1 MPa was measured using an extensometer fixed to the specimen surface. Axial strain in the high-pressure tests was measured either using strain gages mounted to the specimen surface prior to insertion into the pressure vessel or *via* monitoring displacement with a linear variable displacement transducer mounted on the load train and subsequently converting to specimen strain. Calibration curves of axial displacement *vs* specimen strain have been produced at various pressures[37] for the conditions tested. The confining pressures chosen for this study were selected to be less than or comparable to the flow stress of the matrix tested at 0.1 MPa.

The fracture surfaces, in addition to the polished external specimen surfaces, were examined on a JEOL 35CF scanning electron microscope (SEM) operated at 25 KV. Electron fractographic studies of the fracture surfaces were performed to obtain information on the operative fracture modes in the materials deformed under different hydrostatic pressures, while examination of longitudinal sections taken along the specimen axis of failed specimens was conducted to quantify the effects of pressure

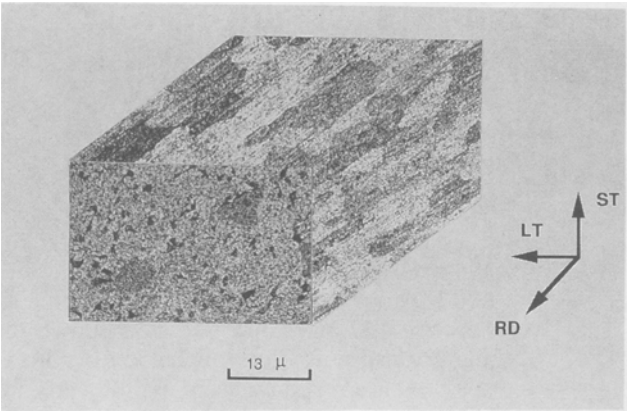

Fig. 1—Optical micrograph of 6061 monolithic material.

on both the nature and extent of the damage (*e.g.*, voids, cracked particles, *etc.*) Scanning electron microscope views were taken on the sectioned and polished specimens along the tensile direction at magnifications of 300 ~ 400 times at distances below the fracture surface from 0.3 to 3.6 mm, in accordance with experiments on ductile fracture in steels conducted by Argon and Im.[38] In total, 12 locations were examined below the fracture surface (Figure 2), while multiple photographs were taken at each location. The distance range chosen here included the necked region (*i.e.*, severely strained) and far from the necked region (*i.e.*, lightly strained). After the SEM examination, each 4″ × 5″ film negative was enlarged to 8″ × 10″ prints for clear identification of voids. A Zeiss videoplan computer with digitizer was additionally used to measure the average size, aspect ratio, and area fraction of voids at each location.

III. RESULTS

The heat treatments described produced nearly identical ductility and the following values of 0.2 pct offset

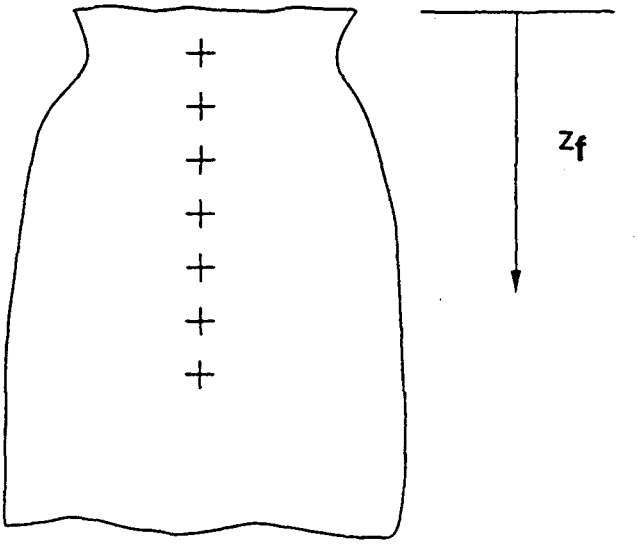

Fig. 2—Schematic showing longitudinal cross section and locations examined which included the necked region (highly strained) and far from the neck (lightly strained).

yield strength at 0.1 MPa: UA = 241 MPa and OA = 264 MPa. Transmission electron microscope views of the UA and OA microstructures are shown in Figures 3 and 4. The UA condition consisted of very fine GP″ + β' precipitates (Mg_2Si), while OA contained platelike β precipitates (Mg_2Si) with an average size of 300 Å. In addition, both UA and OA conditions had nonmetallic inclusions present at the 1.1 vol pct level, with an average size of 3 μm for both the UA and OA conditions. The primary effects of pressure were to increase the ductility, as shown in Figure 5 for both UA and OA conditions. There was no measurable effect of microstructure on the reduction in area (RA) at any of the pressures tested.

Figure 6 illustrates the typical effects of pressure on the macroscopic fracture appearance for both aging conditions. Tests at 0.1 MPa were "double-cup" in appearance, while "chisel point"-type fractures[1–4] were obtained at 150 and 300 MPa for both conditions. The specimens tested under pressure, although extensively deformed and necked, were not circularly symmetric, similar to previous tests on monolithic aluminum reported elsewhere.[1–4] Representative views of the fracture surface morphologies are shown in Figures 7(a) and (b). Equiaxed dimples centered on nonmetallic inclusions (Figure 7(a)) were observed in the 0.1 MPa tests, while smeared fracture surfaces were exhibited in the tests conducted with superimposed hydrostatic pressure (Figure 7(b)). Stereo views taken from Figure 7(b) showed these features to be smeared metal rather than elongated dimples.

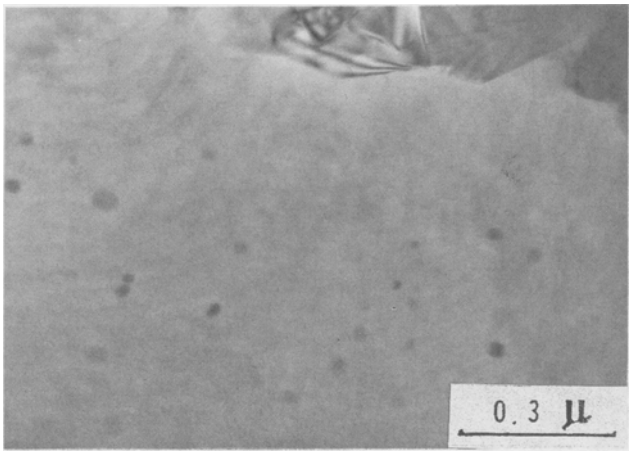

Fig. 3—TEM view of UA microstructure.

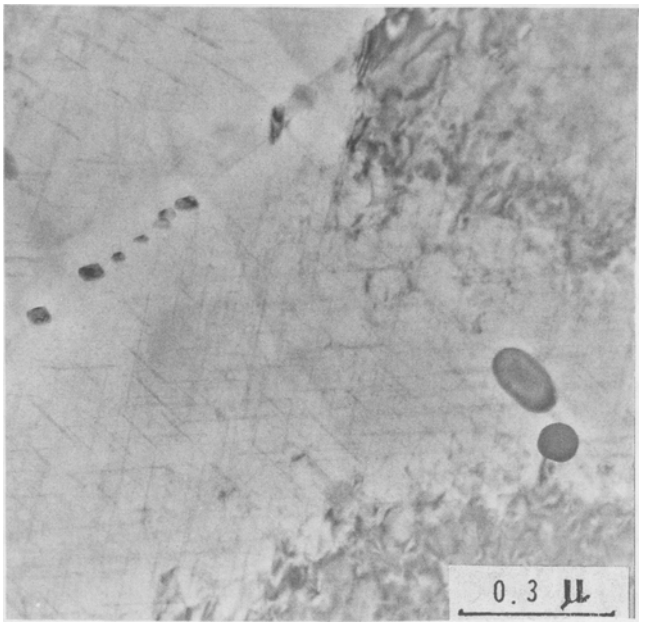

Fig. 4—TEM view of OA microstructure.

Longitudinal sections taken near the fracture surface revealed the presence of voids below the fracture surface of each specimen, as shown in Figure 8. The white particles in Figure 8 are intermetallic inclusions, while the voids centered on these cracked inclusions suggest that the voids were primarily caused by cracking of these inclusions and the subsequent plasticity-driven void growth in the matrix. Tests conducted at 0.1 MPa exhibited voids elongated along the tensile axis direction (Figure 8(a)), while those present at higher pressures were nearly spherical (Figure 8(b)), as shown quantitatively in Figure 9. Measurements of the effects of pressure on the average void size and area fraction of voids at the fracture surface are shown in Figures 10 and 11, respectively. Both figures show that increases in pressure to 150 MPa decrease both the average void size and area fraction, although a further increase in pressure to 300 MPa did not produce much effect, consistent with the similar ductilities obtained at 150 and 300 MPa. Again, little effect of microstructure on the ductility, void fraction, or void size at various pressures is observed for the conditions tested in this material.

Figures 12(a) and (b) show the effects of superimposed pressure on the area fraction of voids in the UA and OA 6061 monolithic materials as a function of normalized distance parameter (Z_f/a_0, where Z_f = distance and a_0 = initial specimen diameter) below the fracture surface. Figures 12(a) and (b) show that the area fraction of voids at the fracture surface (*i.e.*, $Z_f/a_0 = 0$) decreased with increasing superimposed pressure for both

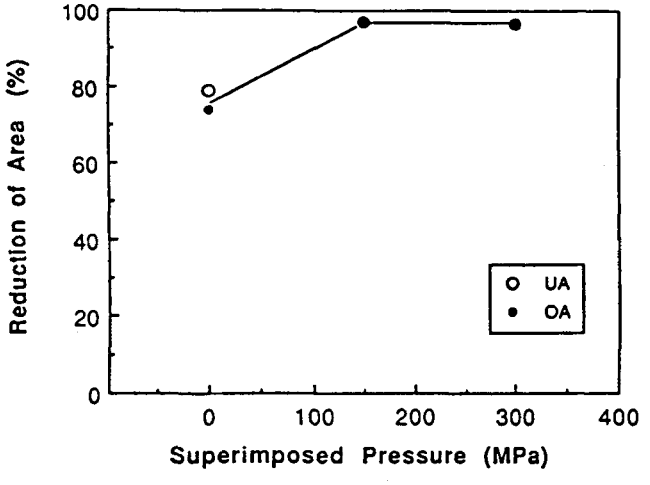

Fig. 5—Effects of pressure on the fracture strain for UA and OA 6061.

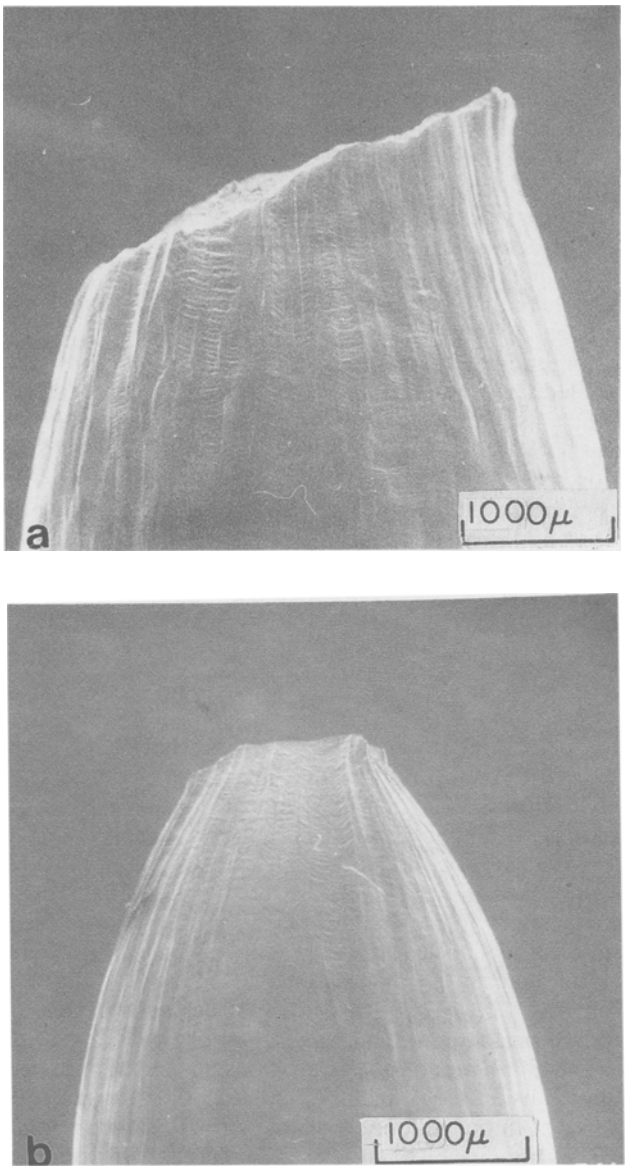

Fig. 6—Macroscopic fracture appearance of 6061 tested at (*a*) 0.1 and (*b*) 300 MPa.

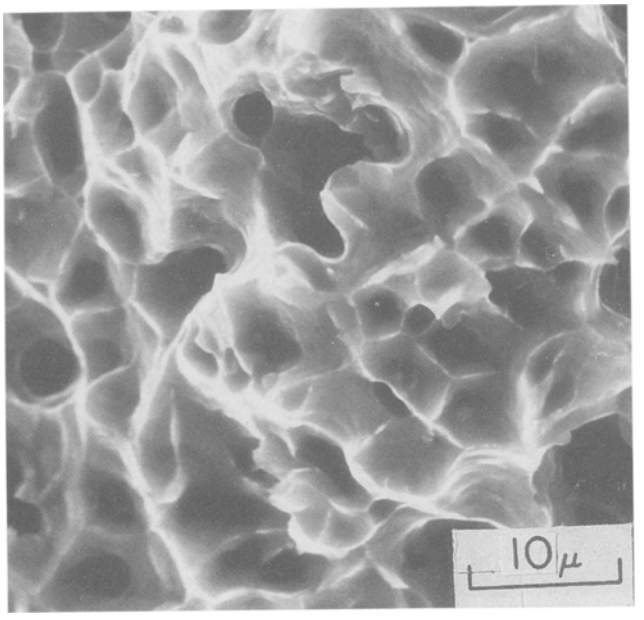

(*a*)

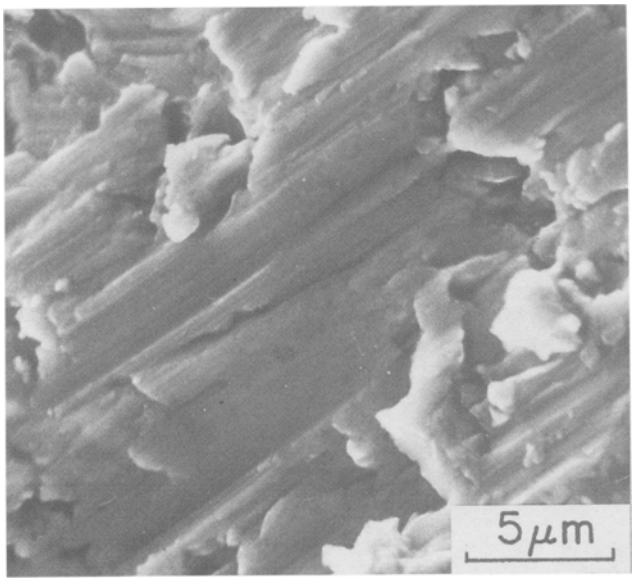

(*b*)

Fig. 7—SEM views of 6061 fracture surfaces: (*a*) 0.1 and (*b*) 300 MPa.

microstructures. Although there is some scatter as one moves below the fracture surface (*i.e.*, $Z_f/a_0 > 0$), the area fraction of voids at a given distance is similar for all pressures tested. Figures 13(a) through (c) compare the effects of matrix microstructure (*i.e.*, UA *vs* OA) on the area fraction of voids in the 6061 monolithic materials tested at 0.1, 150, and 300 MPa superimposed pressure for different distances below the fracture surface. The results again indicate little measurable effect of matrix microstructure on the area fraction of voids below the fracture surface in this material.

The stress-strain curves were nearly identical for all tests at low strains. However, the curves did diverge at higher strains, with significant ductility increases obtained for tests conducted at 150 and 300 MPa. The relative lack of pressure dependence of flow stress at low strains is consistent with other work on similar monolithic aluminum alloys.[24,25,32,39,40]

IV. DISCUSSION

The global effects of superimposed hydrostatic pressure on the ductility of the 6061 aluminum alloy tested presently are similar to those observed by French and Weinrich,[4] where pressure-induced ductility increases were obtained in pure aluminum. However, the present 6061 alloy tested contains a number of additional potential void-nucleating features, such as the precipitates and inclusions identified in Figures 3, 4, 7, and 8. The lack of a significant microstructural effect on ductility at any of the pressures tested (Figure 5), in addition to the observation that the large voids are centered on the nonmetallic inclusions (Figure 7), indicates that the inclusions

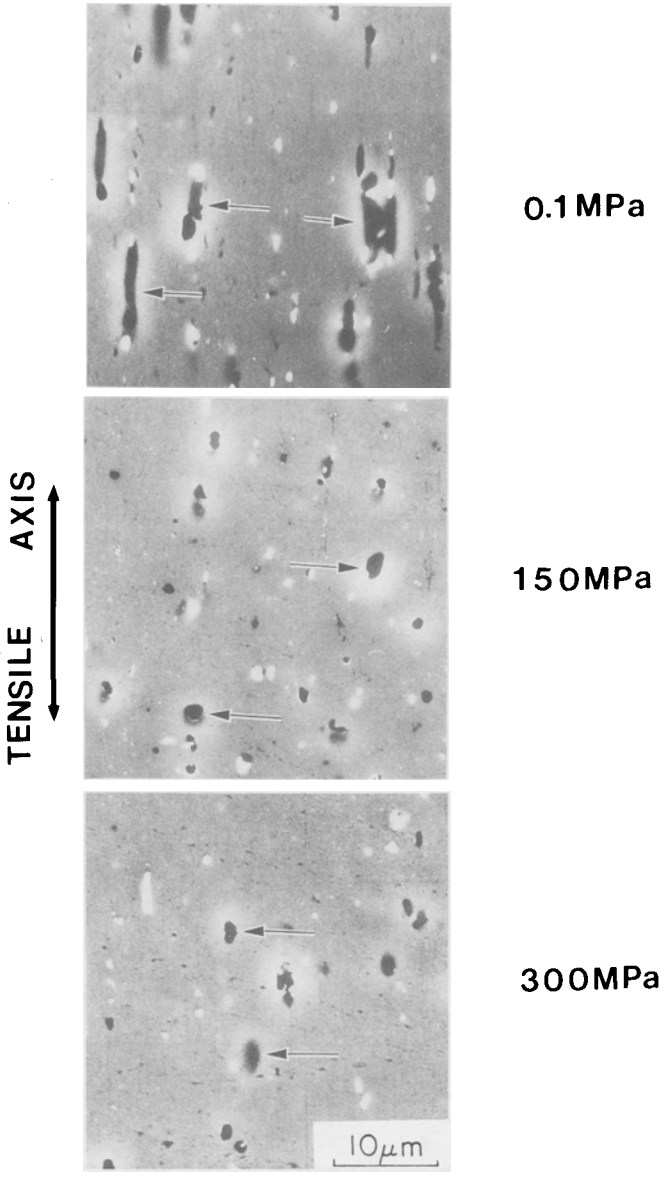

Fig. 8—Appearance of voids adjacent to the fracture surface of specimens fractured at the pressures shown.

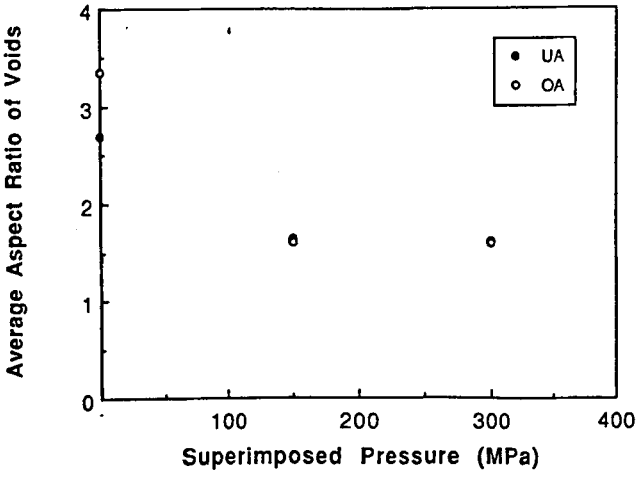

Fig. 9—Effect of pressure on the aspect ratio of voids at the fracture surface.

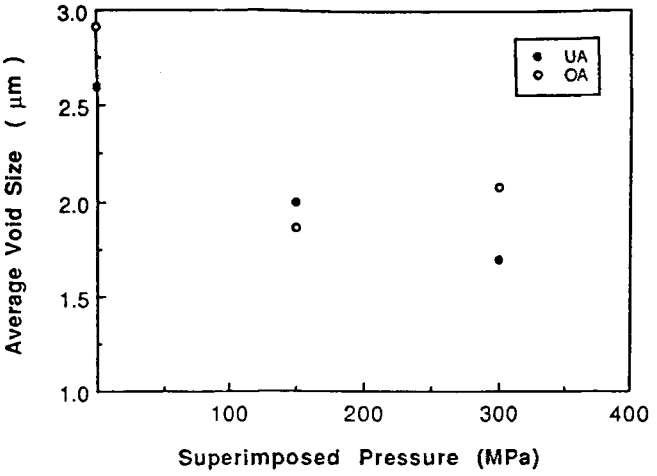

Fig. 10—Effect of pressure on the average void size at the fracture surface.

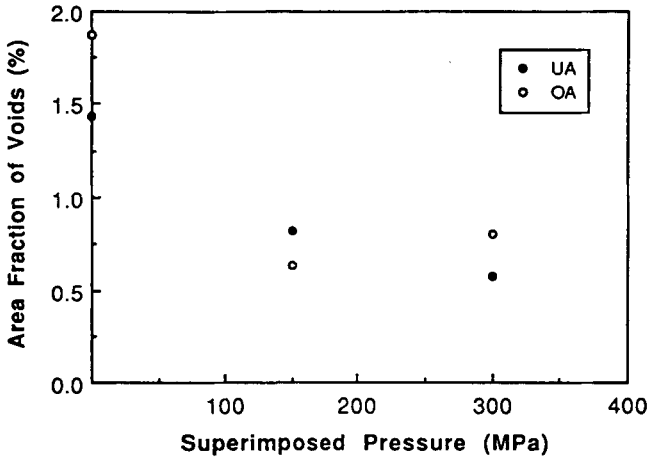

Fig. 11—Effect of pressure on the area fraction of voids at the fracture surface.

are the primary void-nucleating features, at least at low strains. Either complete removal of the inclusions or tests with other aluminum alloys may enable differences between the monolithic UA and OA to be elucidated. For example, recent work on high-strength 7XXX (*i.e.*, Al-Zn-Mg-Cu) and 2XXX (*i.e.*, Al-Mg-Cu) alloys has revealed significant effects of matrix microstructure on the magnitude of pressure-induced ductility increases,[23,24,29] while other work[23,24,29,40] has similarly shown no effect of pressure on ductility of materials which fail by intense localized shear at 0.1 MPa. Examination of the polished longitudinal sections of fractured 6061 specimens indicated that voids were caused primarily by the cracking of inclusions, as shown in Figure 7. These voids were elongated along the tensile axis in specimens tested at atmospheric pressure (Figure 7(a)) and were more spherical in specimens tested at higher pressures (Figure 7(b)). The pressure required to restrict the lengthening of voids corresponds to that at which the fracture mode changes from the double-cup mechanism to the chisel-point mechanism. It is suggested that the

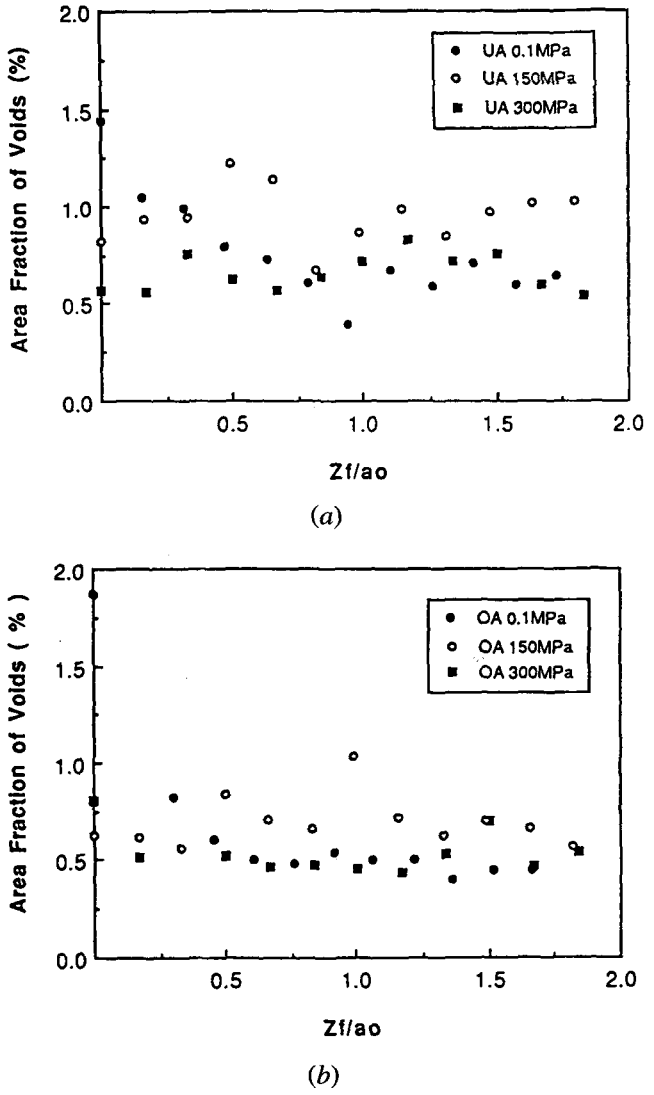

Fig. 12—Effect of pressure on the area fraction of voids in the (*a*) UA and (*b*) OA 6061 material at each distance below the fracture surface, Z_f/a_0, where Z_f = distance below the fracture surface and a_0 = original diameter of specimen.

chisel-point fracture (Figure 6(b)) produced by the localized shear mechanism is the alternative fracture mode when void development is suppressed in the monolithic material by testing under 150 or 300 MPa superimposed pressure.

Figure 11 shows that the area fraction of microvoids observed near the fracture surface is suppressed by superimposed hydrostatic pressure, an indication of pressure-induced inhibition of void growth and coalescence. This is supported by measurements showing the effects of pressure on the absolute number of voids near the fracture surface (Figure 14), where $1/w(dN/dZ)$ is the number of voids per unit area along the tensile axis, w is the width in transverse direction, N is the total number of voids measured, and Z is the length along the tensile axis. Figure 14 shows an increase in the number of voids per unit area for tests conducted at 150 MPa in comparison to those at 0.1 MPa, with a subsequent decrease in number of voids for tests conducted at

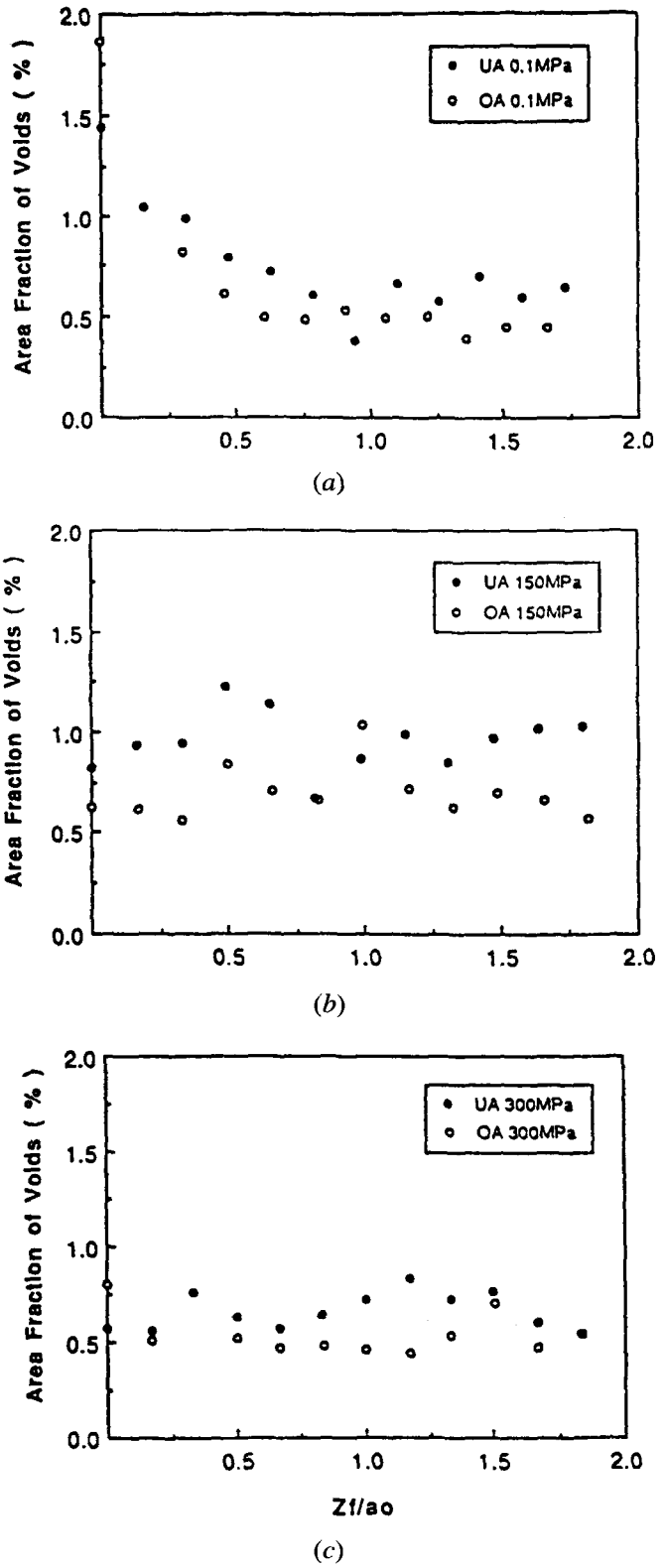

Fig. 13—Effect of pressure on the area fraction of voids at each distance below the fracture surface for (*a*) 0.1, (*b*) 150, and (*c*) 300 MPa.

300 MPa. Re-examination of the void sizes and shapes in Figure 8 provides a plausible rationale for this observation. In tests conducted at 0.1 MPa, the microvoid coalescence occurs at lower strains than that in the high-pressure tests, thereby producing a smaller number of large voids with a high area fraction. As discussed below, superimposed pressure extends the ductility in this system primarily by affecting void growth and coalescence. As such, it appears that the inhibition of void coalescence at 150 MPa produces an increase in the total number of voids, albeit at lower area fraction and size, while higher pressures eventually decrease both the void number and size. Similar effects of pressure on microvoid growth and coalescence were proposed in experiments on copper and brass.[1,2,3]

The pressure levels used presently do not appear sufficient to inhibit microvoid nucleation, which, in this case, primarily occurs via cracking of the inclusions. This is supported by various observations (Figure 12) that the levels of superimposed pressure presently used do not significantly affect the area fraction of voids or the number of cracked inclusions below the fracture surface at every distance. It should be noted that sufficiently high levels of fluid hydrostatic pressure may eliminate or significantly suppress the various mechanisms of microvoid nucleation.[1–5] However, for the more moderate levels of hydrostatic pressures utilized presently, where microvoid nucleation mechanisms are relatively unaffected, it is clear that the subsequent growth and coalescence of microvoids will be strongly influenced by the magnitude of the fluid hydrostatic pressure, as shown in Figures 9 and 10. The results in Figures 9 and 10 are in qualitative agreement with the Rice-Tracey model for void growth,[41] subsequently modified by P.F. Thomason,[42] which predicts an increasing suppression of void growth with increasing hydrostatic pressure. The modified Rice-Tracey model[41,42] predicts that superimposed hydrostatic pressure strongly accentuates the reduction in extensional void growth along the tensile axis while increasing the transverse growth, consistent with the present experimental observations.

It is clear that catastrophic fracture under pressure occurs at significantly higher strains than those obtained at 0.1 MPa. The following analysis was conducted in an attempt to rationalize this behavior and estimate the point of failure under pressure. Specimens were unloaded at various pressure/strain combinations past necking, and the resulting global hydrostatic stress (*i.e.*, due to the neck + superposed pressure) was estimated by the modified Bridgman equations:[5]

$$H = -P + F \ln \frac{r^2 + 2rR}{2rR}$$

where

$$F = \frac{1}{\left(1 + \frac{2R}{r}\right)\left[\ln\left(1 + \frac{r}{2R}\right)\right]} \frac{\text{Load}}{\pi r^2}$$

where P = the hydrostatic pressure;
r = the minimum neck radius; and
R = the radius of curvature of the contour of the neck.

Figure 15 shows the level of hydrostatic stress *vs* strain for tests conducted at 150 MPa. The resultant hydrostatic stress becomes positive at strains exceeding 1.0, while catastrophic fracture occurs at some strain beyond the level at which H exceeds zero. Consistent with previous results on copper and brass,[1,2,3] catastrophic fracture in the high-pressure tests occurs when $H > 0$. In the present tests, it thus appears that the superposition of pressure inhibits microvoid growth and coalescence, particularly past necking.

V. CONCLUSIONS

The effects of low levels of superimposed hydrostatic pressure on the ductility and damage evolution in a 6061 aluminum alloy have been determined as follows:

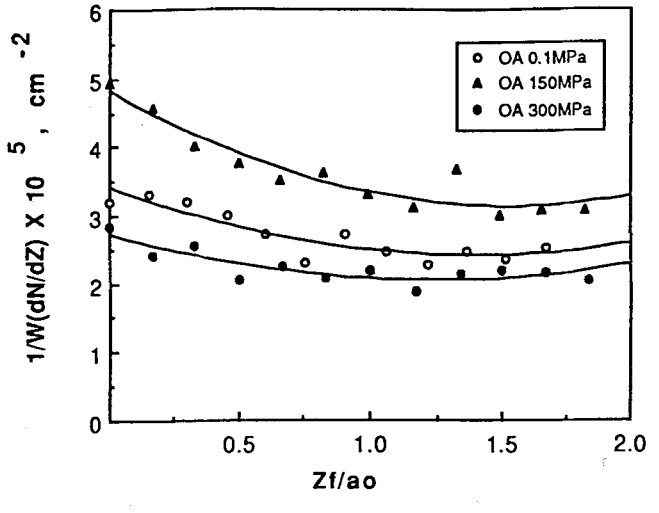

Fig. 14—Effects of pressure on the number of voids per unit length along the tensile axis for each of the pressures tested.

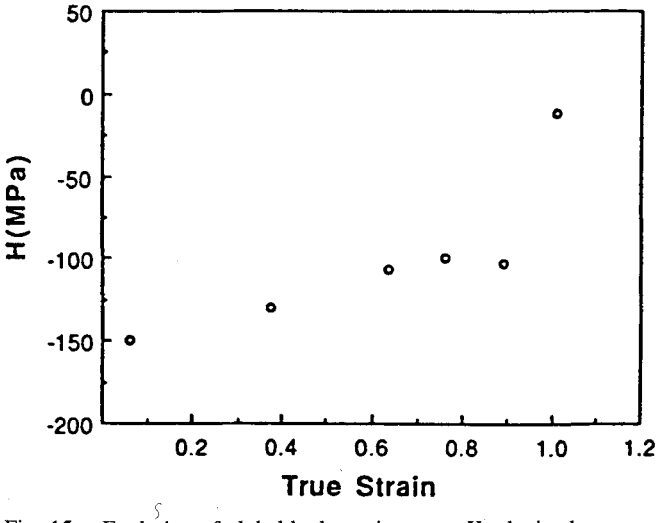

Fig. 15—Evolution of global hydrostatic stress, H, obtained on separate specimens unloaded after testing with 150 MPa pressure to the strains indicated.

1. The ductility at 0.1 MPa and pressure-induced ductility increases for UA and OA 6061 materials were identical. Fracture nucleation occurred primarily at nonmetallic inclusions and did not appear to be affected by the levels of pressure chosen.
2. Microvoid growth and coalescence are significantly suppressed *via* superimposed pressure in the 6061 monolithic materials. Increasing levels of superimposed hydrostatic pressure decreased the average size and aspect ratio of microvoids.
3. Damage evolution at the fracture surface, in terms of area fraction of voids, decreased with increasing superimposed hydrostatic pressure. Little measurable effect of matrix microstructure was observed for the conditions tested in the 6061 monolithic materials.

ACKNOWLEDGMENTS

The authors would like to acknowledge those associated with the High Pressure Facility at Case Western Reserve University and the assistance of B. Goss, C. Liu, and D. Howe. Partial financial support has been provided by ALCAN International Ltd., with additional support from the National Science Foundation, Grant Nos. DMR-89-58326 and ONR-N00014-91-J-1370. Supply of material and technical comments by Dr. D.J. Lloyd of ALCAN is gratefully acknowledged. Useful discussions with M.F. Ashby, J.D. Embury, J.P. Hirth, A.W. Thompson, and J.R. Rice are also gratefully acknowledged.

REFERENCES

1. I.E. French, P.F. Weinrich, and C.W. Weaver: *Acta Metall.*, 1973, vol. 21, pp. 1045-49.
2. I.E. French and P.F. Weinrich: *Metall. Trans. A*, 1975, vol. 6A, pp. 785-90.
3. I.E. French and P.F. Weinrich: *Acta Metall.*, 1973, vol. 21, pp. 1533-37.
4. I.E. French and P.F. Weinrich: *Metall. Trans. A*, 1975, vol. 6A, pp. 1165-69.
5. P.W. Bridgman: *Rev. Modern Phys.*, 1945, vol. 17, pp. 3-14.
6. T.E. Davidson and G.S. Ansell: *Trans. TMS-AIME*, 1969, vol. 245, pp. 2383-90.
7. A. Brownrigg, W.A. Spitzig, O. Richmond, D. Teirlinck, and J.D. Embury: *Acta Metall.*, 1983, vol. 31, pp. 1141-50.
8. W.A. Spitzig: *Acta Metall.*, 1979, vol. 27, pp. 523-34.
9. W.A. Spitzig and O. Richmond: *Acta Metall.*, 1984, vol. 32, pp. 457-63.
10. G.C. Rauch, R.L. Daga, S.V. Radcliffe, R.J. Sober, and W.C. Leslie: *Metall. Trans. A*, 1975, vol. 6A, pp. 2279-87.
11. W.A. Spitzig, R.J. Sober, and O. Richmond: *Metall. Trans. A*, 1976, vol. 7A, pp. 1703-10.
12. S. Yoshida and A. Oguchi: *Trans. JIM*, 1970, vol. 11, pp. 424-30.
13. J.P. Auger and D. Francois: *Int. J. Fracture*, 1977, vol. 13, pp. 431-41.
14. P.F. Weinrich and I.E. French: *Acta Metall.*, 1976, vol. 24, pp. 317-22.
15. F.P. Bullen, F. Henderson, and H.L. Wain: *Phil. Mag.*, 1964, vol. 9, pp. 803-15.
16. F.M.C. Besag and F.P. Bullen: *Phil. Mag.*, 1965, vol. 12, pp. 41-46.
17. A. Ball, F.P. Bullen, and H.L. Wain: *Mater. Sci. Eng.*, 1968, vol. 3, pp. 283-88.
18. E. Aladag, H.Ll.D. Pugh, and S.V. Radcliffe: *Acta Metall.*, 1969, vol. 17, pp. 1467-81.
19. T.E. Davidson, J.C. Uy, and A.P. Lee: *Acta Metall.*, 1966, vol. 14, pp. 937-48.
20. A.W. Christiansen, E. Baer, and S.V. Radcliffe: *Phil. Mag.*, 1971, vol. 24, pp. 451-67.
21. R. Margevicius and J.J. Lewandowski: *Scripta Metall.*, 1991, vol. 25, pp. 2017-22.
22. J.J. Lewandowski, C. Liu, and W.H. Hunt, Jr.: *Powder Metallurgy Composites*, M. Kumar, K. Vedula, and A.M. Ritter, eds., TMS-AIME, Warrendale, PA, 1987, pp. 117-39.
23. D.S. Liu, M. Manoharan, and J.J. Lewandowski: *Metall. Trans. A*, 1989, vol. 20A, pp. 2409-17.
24. D.S. Liu, M. Manoharan, and J.J. Lewandowski: *Scripta Metall.*, 1989, vol. 23, pp. 253-56.
25. J.J. Lewandowski, D.S. Liu, and C. Liu: *Scripta Metall.*, 1991, vol. 25, pp. 21-26.
26. R.W. Margevicius and J.J. Lewandowski: *Scripta Metall. Mater.*, 1992, vol. 26, pp. 1733-36.
27. R.W. Margevicius and J.J. Lewandowski: *Acta Metall. Mater.*, 1993, vol. 41, pp. 485-96.
28. J.J. Lewandowski, G.M. Michal, I. Locci, and J.D. Rigney: in *Proc. MRS Symp.*, G.M. Stocks, A. Giamei, and D. Pope, eds., MRS, Pittsburgh, PA, 1990, vol. 186, pp. 341-48.
29. D.S. Liu, M. Manoharan, and J.J. Lewandowski: *J. Mater. Sci. Lett.*, 1989, vol. 8 (12), pp. 1447-48.
30. J.J. Lewandowski, C. Liu, and W.H. Hunt, Jr.: *Mater. Sci. Eng.*, 1989, vol. A107, pp. 241-55.
31. D.J. Lloyd: *Acta Metall.*, 1991, vol. 39, pp. 59-71.
32. F. Zok, J.D. Embury, M.F. Ashby, and O. Richmond: *9th Risø Int. Symp. Metallurgy and Materials Science*, S.I. Anderson, H. Lilhot, and O.B. Pederson, eds., Risø National Laboratory, Denmark, 1989, pp. 517-27.
33. A.K. Vasudevan, O. Richmond, F. Zok, and J.D. Embury: *Mater. Sci. Eng.*, 1989, vol. A107, pp. 63-69.
34. T. Christman, A. Needleman, J. Nutt, and S. Suresh: *Mater. Sci. Eng.*, 1989, vol. A107, pp. 49-60.
35. C.P. You, A.W. Thompson, and I.M. Bernstein: *Scripta Metall. Mater.*, 1987, vol. 21, pp. 181-87.
36. D.S. Liu and J.J. Lewandowski: *Metall. Trans. A*, 1993, vol. 24A, pp. 609-15.
37. D.S. Liu and R.W. Margevicius: Case Western Reserve University, Cleveland, OH, unpublished research, 1991.
38. A.S. Argon and J. Im: *Metall. Trans. A*, 1975, vol. 6A, pp. 839-51.
39. D.S. Liu, R.W. Margevicius, and J.J. Lewandowski: *Proc. 2nd Int. Ceramic Science and Technology Congress—Advanced Composite Materials*, M.D. Sacks, ed., The American Ceramic Society, Inc., Westerville, OH, 1990, pp. 513-18.
40. A. Korbel, V.S. Rangunathan, D. Teirlinck, W. Spitzig, O. Richmond, and J.D. Embury: *Acta Metall.*, 1984, vol. 32, pp. 511-19.
41. J.R. Rice and D.M. Tracey: *J. Mech. Phys. Solids*, 1969, vol. 17, p. 201.
42. P.F. Thomason: *Ductile Fracture of Metals*, Pergamon Press, Oxford, United Kingdom, 1990.